J Mater Sci (2007) 42:8804–8810
DOI 10.1007/s10853-007-1916-z

A solid-state NMR comparison of the mineral structure in bone from diseased joints in the horse

Sergey Maltsev · Melinda J. Duer · Rachel C. Murray · Christian Jaeger

Received: 19 December 2006 / Accepted: 4 June 2007 / Published online: 10 July 2007

Abstract In this work, subchondral cortical bone material is investigated from the joints of five horses, three of which presented with no clinical signs or radiographic signs of osteoarthritis and two of which suffered osteoarthritis joint disease, as judged by clinical and radiographic assessment and histological findings. The horse is a good model for osteoarthritis in humans, so the aim of this study is to use nuclear magnetic resonance (NMR) for a detailed investigation of the bone structure in bone material affected by osteoarthritis. In particular, we report on the assessment of the mineral structure of these samples as viewed by solid-state NMR.

Introduction

Bone as a material is interesting from a number of points of view. From the biological perspective, it is the material which gives higher animals their shape and form and allows locomotion. From the materials science perspective, it is an organic–inorganic composite material which exhibits remarkable strength and resilience to fracture under most circumstances. Increasingly, the structure of bone on molecular length scales has been studied in order to understand its material properties in more detail and so to generate a design template for new synthetic materials mimicking its properties.

Bone is known to fail as a material under some instances. Trauma generated fractures are common, as is repetitive overloading injury in athletes. The bone diseases of osteoporosis and osteoarthritis (OA) have huge economic and welfare impact in the human population. In the case of osteoporosis, the material strength of the bone is clearly compromised. However, the effect of osteoarthritis on the integrity of bone material is less well understood. An osteoarthritis-associated increase in subchondral bone volume and trabecular thickness has been detected in subchondral cortical and cancellous bone from a number of species [1–4]. An increase in bone mineral density has been associated with osteoarthritis in human joints [5] and it appears that osteoarthritis is less likely in osteoporotic individuals [5–7]. However, although increased remodeling of subchondral bone in osteoarthritis has been indicated in a number of reports [2, 3, 8–10], hypomineralization of subchondral bone has also been noted [2, 11]. It is reported that the stiffness of subchondral cancellous bone increases in osteoarthritis [12, 13], while the stiffness of subchondral cortical bone decreases [14–16]. It is clear from these various reports that bone mineral structure plays a part in osteoarthritis, though less clear how. Accordingly, we have undertaken a solid-state NMR study in order to characterize the bone mineral in osteoarthritis, in order to improve our understanding of the molecular basis of the disease.

Solid-state NMR is an ideal method for studying composite materials such as bone. An NMR spectrum for a

S. Maltsev · C. Jaeger (✉)
Federal Institute for Materials Research and Testing, Division I.3, Working Group NMR Spectroscopy, Richard Willstaetter Str. 11, D-12489 Berlin, Germany
e-mail: christian.jaeger@bam.de

M. J. Duer
Department of Chemistry, University of Cambridge, Lensfield Road, Cambridge CB2 1EW, UK

R. C. Murray
Centre for Equine Studies, Animal Health Trust, Lanwades Park, Kentford, Newmarket, Suffolk CB8 7UU, UK

particular nuclear isotope contains signals from all such nuclear spins in the sample, distinguished by their chemical shift, which is determined by the chemical environment of the spin. Moreover, experiments can be designed such that through-space magnetic dipole–dipole interactions between nuclear spins also affect the spectrum in some measurable manner. The dipole–dipole coupling between nuclear spins has a strength which is proportional to $1/r^3$ where r is the internuclear distance. Thus, experiments can be performed in which different chemical sites can be distinguished by the different frequencies of the signals arising from them and for each such site distinguished, its spatial correlation to other nuclear spins determined. The signals from nuclear spins also relax over time, with a characteristic time constant which is determined by the environment of the spin; measurement of such relaxation times thus often provides useful information on molecular-level structure as well. In this study we will use the dipole–dipole coupling between ^{1}H and ^{31}P spins to perform heteronuclear correlation (HETCOR) experiments which examine the ordering and disposition of phosphate, hydroxide and water in the mineral component of the bone samples of interest. ^{1}H and ^{31}P spin-lattice (T_1) relaxation time measurements are used to further characterize these species and their environment.

The horse is a good model for osteoarthritis in humans [9], so the aim of this study was to use equine subchondral cortical bone to investigate the hypothesis that mineral structure and composition is altered in osteoarthritis compared to normal bone. The objective of the study was to use solid state NMR to compare mineral composition and structure between subchondral bone from horses with and without clinical, radiographic and histological evidence of osteoarthritis.

Experimental

Samples

Osteochondral samples from the dorsal proximal aspect of the third tarsal bone were obtained from five horses following humane destruction for clinical reasons unrelated to this study. Three horses had no clinical, radiographic or histological evidence of abnormality or pain (samples 27, 82, 85, aged 3, 6 and 7 years, respectively). Two horses had clinical signs of pain localized to the tarsometatarsal joint with radiographic and histological evidence of osteoarthritis (samples 64 and 124, aged 10 and 17 years).

Naturally-hydrated samples were frozen in liquid nitrogen and ground in a Sartorius Dismembrator ball mill. The samples were then immediately transferred via a funnel into the NMR rotors (approximately 100 mg) and lightly pressed into place with a plastic rod.

NMR

The measurements were performed on BRUKER Avance 600 spectrometer, operating at 600 MHz for ^{1}H and 243 MHz for ^{31}P using a magic-angle spinning (MAS) probe which utilized 4 mm zirconia rotors. The spinning frequency was 12.5 kHz for all experiments. The 90° ^{1}H and ^{31}P pulse length were 3 μs and 5 μs, respectively. The ^{1}H echo experiments were acquired with an echo delay of single rotor period (80 μs) and a spectral width of 100 kHz. The relaxation delay was 2s.

For the ^{1}H–^{31}P cross polarization measurements (CP) a recycle delay of 2 s was used, and the ^{1}H spin-lock field was ramped down to 50% to broaden the match condition.

Two-dimensional ^{1}H–^{31}P heteronuclear correlation (HETCOR) experiments [17] were performed using frequency-switch Lee-Goldburg (FSLG) [18] cross polarization (CP) with contact times of 100 μs, 200 μs, 300 μs, 500 μs, 750 μs, 1 ms, 2 ms, 4 ms, 6 ms and 8 ms. A total of 64 scans were averaged for each t_1 time increment in the two-dimensional experiment.

^{1}H T_1 relaxation time measurements of the proton species in the mineral crystals cannot be done directly, because most of the protons are located in the organic matrix such that these signals must be suppressed. Hence, the overall ^{1}H T_1 "mineral" time can be measured either by detecting the ^{31}P signal after CP and varying the ^{1}H relaxation delay after presaturation before CP or using a ^{1}H echo sequence prior to the T_1 experiment. In the latter case the protons in the protein matrix dephase and only ^{1}H nuclei of the mineral phase remain. The relaxation delays were 50 ms, 100 ms, 200 ms, 500 ms, 1 s, 2 s, 5 s, 10 s, 20 s and 50 s using eight scans for each measurement.

Finally, the ^{31}P T_1 relaxation times were determined using the Torchia method [19] after cross polarization. The delays were varied from 1 s to 2,800 s.

Histology

Osteochondral samples underwent routine histological preparation, decalcification and paraffin-embedding. Four μm thick sections were stained with Toluidine blue and Haematoxylin and Eosin for evaluation of the articular cartilage and subchondral bone. Cartilage morphology was assessed using an Olympus DP12 microscope (Olympus UK Ltd., London, UK) and a polarized light. Each section was assessed with respect to chondrocyte orientation and morphology, staining patterns, articular surface and osteochondral junction defects; focal cartilage and subchondral bone abnormalities; cartilage erosion; osteophyte formation; abnormally increased area of dense bone and focal cancellous bone abnormalities. Presence of osteoarthritic change was based on previously described histo-

logical scoring systems for cartilage and subchondral bone [20, 21].

Results and discussion

Histology

Samples 27, 82 and 85 had no evidence of osteoarthritic change in either the cartilage or subchondral bone at any site within the joint. Samples 64 and 124 had clear evidence of osteoarthritic change within this joint cartilage structural disorganization with chondrone formation and subchondral bone fibrosis. Sample 64 had clear definition of the subchondral bone margins. Sample 124 had marked thickening of the subchondral bone with generalized loss of porosity, typical of osteoarthritic changes (Fig. 1).

NMR

Fig. 2 shows the two-dimensional ^{1}H–^{31}P HETCOR spectra for samples 27 and 64 as typical samples from the non-OA and OA groups. The spectra were recorded using FSLG (frequency switched Lee-Goldburg) cross polarization and ^{1}H–^{31}P mixing times of 0.5 ms, 2 ms and 8 ms. These spectra show the spatial correlations between ^{1}H spins (from various groups) and ^{31}P spins (primarily phosphate species contained in the mineral component) in the sample, and so essentially contain information about the spatial correlation of ^{1}H containing groups in the mineral/closely bound to the mineral surface and mineral phosphate, there being little phosphate elsewhere in the bone matrix observable by NMR [22]. As most of the protons (^{1}H) of the protein matrix are not close to ^{31}P, the protons in the protein matrix are not observed in this experiment, making it an excellent method by which to examine the mineral component of a sample exclusively, without resorting to deproteination of the sample, as discussed previously by Ackermann et al. [22].

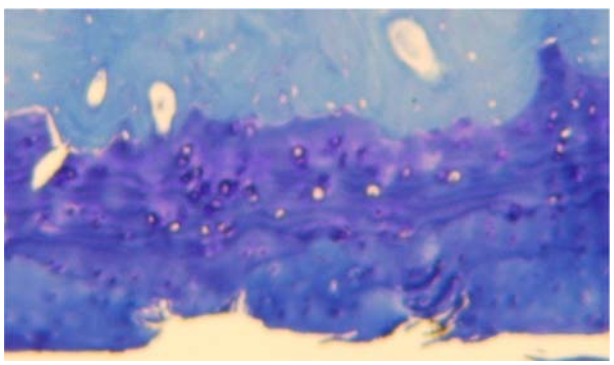

Fig. 1 Stained microscopy of the osteoarthritic sample 124

The spectra shown in Fig. 2 for the two different samples are very similar in both ^{1}H and ^{31}P lineshapes and in the relative intensities of the various signals to each other for equivalent mixing times. Moreover, they are similar to those reported previously by other workers examining the mineral structure of bone from bovine and rat species [23], and bovine, rat and human [22]. Very similar spectra are found for all the other samples in this work and results from experiments which used Hartmann–Hahn cross polarization rather than FSLG are similar also (a loss of the water signal due to spin-diffusion processes can occur in Hartmann–Hahn experiments). The latter is not surprising as ^{1}H–^{1}H distances in the mineral matrix are expected to be large so that at the MAS frequency (12.5 kHz), spin diffusion between ^{1}H spins is expected to be slow on the timescale of the cross polarization transfer and under such circumstances, the cross polarization dynamics are similar for FSLG and Hartmann–Hahn cross polarization.

The spectra in Fig. 2 show at least three broad signals in the ^{1}H dimension: a sharper signal at approximately 0 ppm, due to OH^- hydroxyl ions, a broad peak centered around 5.5 ppm due to structural water in the mineral (or at least, water in close proximity to mineral phosphate, otherwise this signal would not appear in the spectrum at all) and a very broad peak in the region 5–15 ppm from HPO_4^{2-} hydrogen phosphate groups. The OH^- ^{1}H signal is correlated with a relatively narrow ^{31}P resonance, indicating that the phosphate groups in close spatial proximity to the hydroxyl groups are relatively well ordered, and thus belong to a relatively crystalline hydroxyapatite structure. The H_2O and HPO_4^{2-} ^{1}H signals, on the other hand, are correlated with relatively broad ^{31}P lines, indicating that these ^{1}H and their nearby phosphate/hydrogen phosphate groups are in relatively disordered environments.

Two-dimensional ^{31}P–^{31}P correlation spectra for the samples under non-spinning conditions for mixing times of 1 ms, 10 ms, 100 ms, 1 s and 10 s and room temperature (not presented in this paper) were undertaken to establish whether all mineral crystals are similar or whether there are populations with different species of phosphate groups. At short mixing times, the exchange pattern in the two-dimensional spectrum is simply a diagonal lineshape as there is essentially no spin diffusion between the ^{31}P spins on this timescale. As the mixing time increases, there are increasing amounts of exchange intensity correlating different ^{31}P signals, until at mixing times of 1 s and above, the exchange pattern is essentially circular, indicating that all ^{31}P signals are correlated with each other. Moreover, the buildup of exchange intensity with mixing time to this position is smooth. In other words, all the ^{31}P sites represented in these spectra (and therefore, also the HETCOR spectra in Fig. 2) exist in every crystallite in the sample, i.e. the different ^{1}H sites and phosphate groups inferred

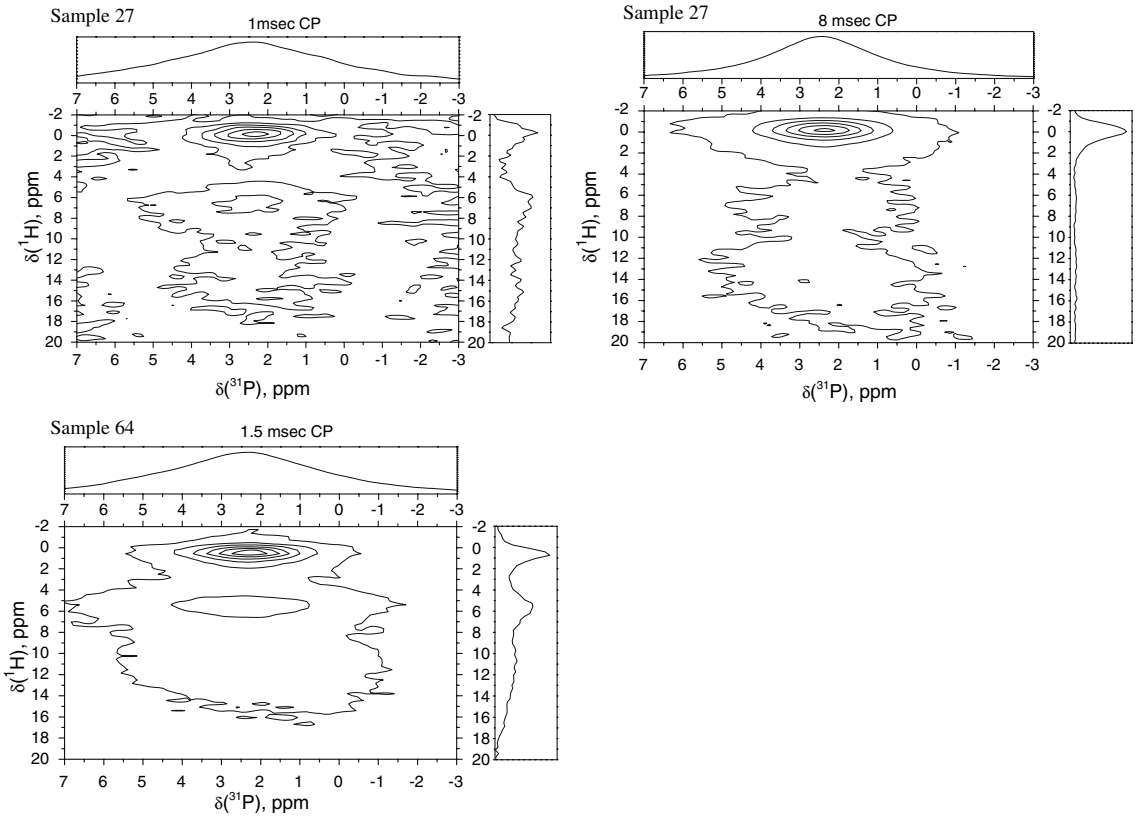

Fig. 2 2D ^{1}H–^{31}P FSLG HETCOR for sample 27 and sample 64 at mixing times of 1 ms and 1.5 ms respectively and sample 27 at mixing times of 8 ms

from the HETCOR spectra in Fig. 2 exist in every crystallite; there are not different mineral phases in different crystallites for instance.

We thus ascribe the more disordered region containing H_2O/phosphate and HPO_4^{2-} groups to surface regions of the crystallites and the more ordered OH^-/PO_4^{3-} groups to a more crystalline core in the crystallites as it was shown recently for nanocrystalline hydroxyapatite in detail [22]. This is consistent with the idea that the surface regions of any crystal are expected to be more disordered due to the lack of coordination around surface ions, and/ or coordination of surface ions by heterogeneous molecules from the protein matrix in the case of mineral crystals in bone. The H_2O/phosphate region may arise in part or whole from matrix water bound to the surface of the mineral crystallites.

HETCOR spectra in Fig. 2 were recorded in fact for between four and ten mixing times for each sample. This allows us to determine the approximate rate constants for the (presumed exponential) build up of ^{31}P magnetization by cross polarization from ^{1}H, which in turn depends on the ^{1}H–^{31}P distances involved, as well as other interactions affecting both the ^{1}H and ^{31}P spins and any local molecular dynamics (for instance, local rotations or librations of water molecules).

The rate constants were determined by fitting the experimental data to Eq. (1) [24].

$$S(t) = a[1 - \exp(-t/\tau_{HP})]\ \exp(-t/\tau_d) \quad (1)$$

where $S(t)$ is the ^{31}P signal intensity for a mixing time of t, τ_{HP} is the rate constant for the ^{1}H–^{31}P cross polarization process and τ_d is a decay constant describing the decay of the ^{31}P signal through various relaxation processes affecting both the ^{1}H and ^{31}P spins.

The τ_{HP} rate constants determined for the ^{31}P signal intensity in the three regions indicated in Fig. 3 are given in Tables 1 and 2 for HETCOR spectra using Hartman–Hahn and FSLG cross polarization, respectively.

It should be noted that τ_{HP} for the OH^-/PO_4^{3-} region is difficult to determine accurately due to the near linear profile of the signal buildup for the ^{31}P intensity in this spectral region over the range of mixing times used.

The data in Tables 1 and 2 shows that the τ_{HP} rate constants for each ^{31}P spectral region are very similar within the limits of error for all samples studied. This, plus the similarity of the two-dimensional HETCOR spectra themselves leads us to conclude that the mineral compositions and structures are very similar for all samples and

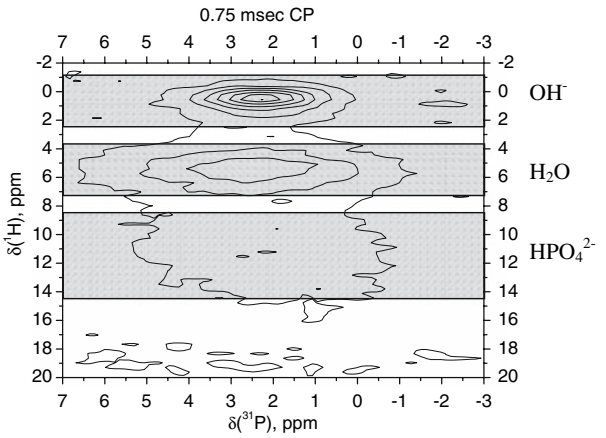

Fig. 3 OH^-, water and HPO_4^{2-} ^1H spectral assignment on the ^1H–^{31}P correlation spectra

Table 1 The rate constants τ_{HP} for the ^{31}P intensity in the three spectral regions shown in Fig. 2 of ^1H–^{31}P HETCOR spectra recorded using Hartman–Hahn cross polarization

Sample	τ_{HP} (OH^-/PO_4^{3-} region)/ms	τ_{HP} (H_2O/PO_4^{3-} region)/ms	τ_{HP} (HPO_4^{2-} region) /ms
27	2.9 ± 0.5	0.6 ± 0.1	0.4 ± 0.2
64	10 ± 4	0.6 ± 0.1	0.6 ± 0.1
124	2.6 ± 0.8	0.7 ± 0.1	0.6 ± 0.2

Error estimates are from curve fitting and do not take direct account of experimental errors

Table 2 The rate constants τ_{HP} for the ^{31}P intensity in the three spectral regions shown in Fig. 2 of ^1H–^{31}P HETCOR spectra recorded using FSLG cross polarization

Sample	τ_{HP} (OH^-/PO_4^{3-} region) /ms	τ_{HP} (H_2O/PO_4^{3-} region)/ms	τ_{HP} (HPO_4^{2-} region)/ms
64	1.7 ± 0.3	0.5 ± 0.1	0.4 ± 0.1
124	2 ± 1	0.3 ± 0.1	0.2 ± 0.2

Error estimates are from curve fitting and do not take direct account of experimental errors

thus that joint disease has not changed the mineral structure in any way that we can measure here.

It is interesting to examine the ^{31}P lineshapes extracted from the two-dimensional HETCOR spectra in Fig. 2. These are plotted for sample 27 in Fig. 4 for different ^1H–^{31}P FSLG mixing times for the three spectral regions indicated in Fig. 3. Other samples give near identical plots, indicating that the phosphate environment and distribution is very similar in all samples. The ^{31}P lineshape for the OH^-/PO_4^{3-} spectral region is invariant with mixing time in both the FSLG and Hartman–Hahn mixing time experiments. This is the behaviour expected for a single component (crystalline) system in which there is one type of PO_4^{3-} in spatial proximity to one type of OH^-; hydroxyapatite.

The ^{31}P lineshape for the H_2O/ phosphate region shows more complex behaviour: an initially broad ^{31}P lineshape *decreases* in linewidth as the mixing time increases from 2 ms to the longest mixing time studied, 8 ms, for both FSLG and Hartman–Hahn mixing (the latter not shown). One possible explanation for this effect is that at the longer

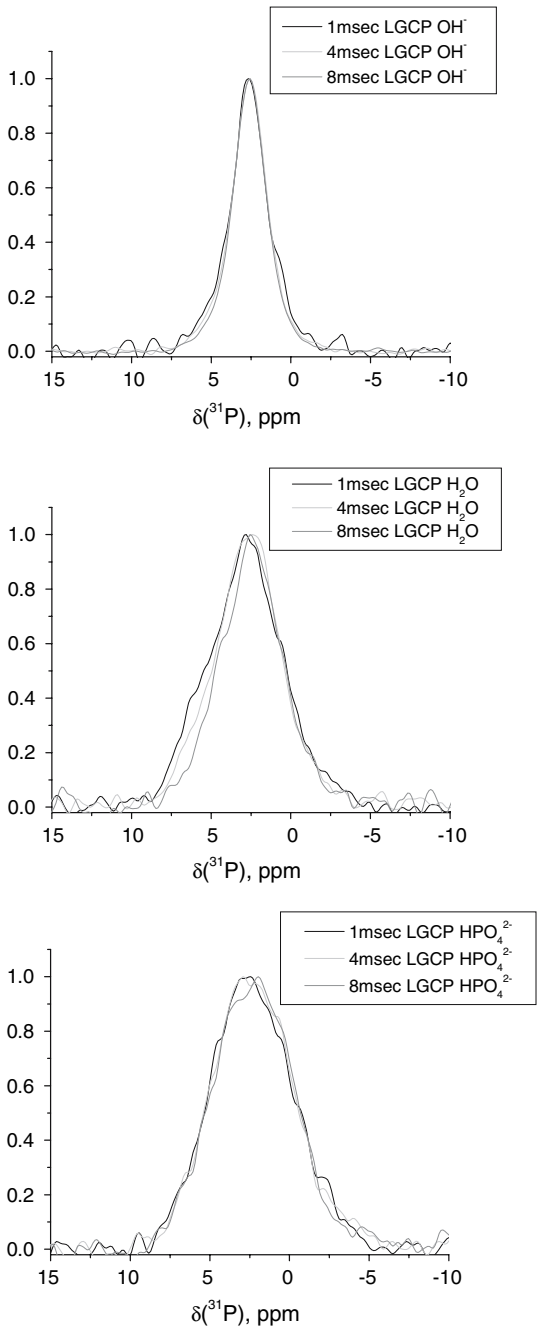

Fig. 4 The ^{31}P lineshapes extracted from the two-dimensional FSLG HETCOR spectra for the three spectral regions defined in Fig. 2 for sample 27 for FSLG mixing times of 1–8 ms

mixing times, there is spin diffusion from H_2O ^1H to OH^- groups in the ordered hydroxyapatite regions somewhere in the experiment prior to cross polarization to ^{31}P, so that magnetization which initially started on H_2O ends up on the ordered phosphate groups (and ^{31}P spins thereof) in the hydroxyapatite core of the crystallites. However, FSLG mixing does not permit spin diffusion between ^1H spins during the mixing period and the longest t_1 time used in the HETCOR experiment is 6 ms which from previous work [25] is too shorter a time for there to be significant spin diffusion between ^1H spins (significant spin diffusion between OH^- and H_2O only occurs on a timescale of 200 ms [25]). Thus, the existence of the narrowed ^{31}P line does not arise from spin diffusion between ^1H, but must instead arise from a second phosphate site spatially correlated with H_2O which has different cross polarization dynamics to the sites which account for the main cross polarization events at shorter mixing times. The fact that this second site does not become apparent until longer mixing times suggests that either (a) its cross polarization transfer rate constant τ_{HP} is significantly longer, or (b) the decay constant governing the decay of the ^{31}P cross polarization signal is significantly less than, those for the sites which account for the majority of polarization transfer at short mixing times. Alternatively, both (a) and (b) may occur to some extent. In case (a), the conclusion would be that the H_2O from which the cross polarization is occurring for this second H_2O/phosphate site is relatively distant from the phosphate to which it cross polarizes and in case (b), that the rotating-frame spin-lattice relaxation times for the ^{31}P and/or ^1H involved in the cross polarization process for the second H_2O/phosphate site are significantly smaller than for other H_2O/phosphate groups with the faster cross polarization rates. Moreover, the phosphate groups involved in this second site are (from the narrowed ^{31}P lineshape) more ordered than for the rapidly cross polarizing H_2O/phosphate sites. A likely explanation is that the mineral bone crystals consists of crystalline hydroxyapatite as core covered with an amorphous layer as found for nanocrystalline hydroxyapatite [23]. It must then be concluded that the water molecules are close to this interface which in turn would explain the higher degree of order of the phosphate anions due to the near hydroxyapatite structure.

For completeness in this study, we have recorded the mineral ^1H and ^{31}P T_1 relaxation time constants for each sample also. These are shown in Table 3. It should be noted that a single T_1 time constant describes the relaxation of the entire ^1H spectrum within experimental error. The estimates of error are estimates of the error from fitting the experimental data points to an exponential curve. They do not take into account noise in the experimental data nor the effects of any baseline errors (for instance) in the experimental data. Thus, from the values in Table 3, we believe that the T_1 values for both mineral ^1H and ^{31}P are very similar between all samples once all sources of error are taken into account. Two methods were used for determining the T_1 values: (1) direct T_1 measurements, after first selecting the mineral ^1H spectroscopically (which is done here using a rotor-synchronized echo; the protein ^1H signals have relatively short transverse relaxation times and so decay during the echo period, leaving only the mineral ^1H signal at the end of the echo experiments), and (2) indirect measurement using cross polarization from ^1H to ^{31}P (which automatically selects the mineral ^1H, as only these are close enough to ^{31}P spins to cross polarize). In first case, we obtain relaxation information of every ^1H signal independently. In the second case, we obtain the information about ^1H relaxation through the ^{31}P nuclei. In general, the T_1 relaxation times measured in these two ways can be different. The difference tells us about the internal structure of proton lines: if, for example, T_1 relaxation measured via cross polarization to ^{31}P is faster, then there are at least two components forming the ^1H line and this should be taken account of when analyzing the experimental relaxation data. However, T_1 values measured by methods (1) and (2) were very similar, strongly suggesting that a one exponent analysis is sufficient.

Table 3 The ^1H and ^{31}P T_1 relaxation time constants for the bone samples used in this work. The measurement method is described in the *Experimental* section

Sample	27	82	85	64	124
^1H T_1/s	1.1 ± 0.3	1.1 ± 0.2	1.0 ± 0.2	1.1 ± 0.2	1.2 ± 0.3
^{31}P T_1/s	244 ± 4	207 ± 3	213 ± 3	228 ± 3	206 ± 6

Furthermore, in our work, using different cross polarization contact times (100 μs and 9 ms) yields very similar T_1 behaviour, despite the fact, that for a 100 μs contact time, there is almost no signal from hydroxyapatite OH^- ^1H present in the spectrum and at 9 ms, almost no HPO_4^{2-} or H_2O signal contributes to the spectra. This further suggests that one exponent fitting of the experimental T_1 relaxation curves may be used and, within error limits, this gave acceptable fits in every case.

Conclusions

We have investigated the molecular-level structure of the mineral in bone taken from the subchondral regions of equine joints where there was clinical and histological evidence of OA joint disease. Our study used solid-state NMR as the primary method of structure investigation and we employed a number of different experiments including two-dimensional ^1H-^{31}P HETCOR spectra and relaxation

time measurements. Our results do not find any differences between the mineral structure and composition of the diseased bone samples as compared with bone which from clinical findings and histology is not diseased. This suggests that the osteoarthritis may have more influence on the bone organic matrix or its interaction with the mineral, than alteration in the mineral structure itself. These results will no doubt add to the debate about how precisely OA affects underlying bone structure and strength.

References

1. Dequeker J, Mokassa L, Aerssens J, Boonene S (1997) Microsc Res Tech 358:37
2. Grynpas MD, Alpert B, Katz I, Lieberman I, Pritzker KPH (1991) Calcif Tissue Int 20:49
3. Panula HE, Nieminen J, Parkkinen JJ, Arnala I, Kroger H, Alhava E (1998) Acta Orthop Scand 627:69
4. Radin EL, Martin BM, Burr DB, Caterson B, Boyd RD, Goodwin J (1984) J Orthop Res 221:2
5. Burr DB (1998) Curr Opin Rheumatol 256:10
6. Burr DB, Schaffler MB (1997) Microsc Res Tech 37:343
7. Dequeker J (1985) Clin Rheum Dis 271:11
8. Matsui H, Shimizu M, Tsuhi H (1997) Microsc Res Tech 333:37
9. Murray RC, Vedi S, Birch HL, Lakhani KH, Goodship AE (2001) J Orthop Res 1035:19
10. Shimizu M, Tsuji H, Matsui H, Katoh Y, Sano A (1993) Clin Orthop 229:293
11. Mansell JP, Bailey AJ (1998) J Clin Invest 1596:101
12. Finlay JB, Bourne RB, Kraemer WJ, Moroz TK, Rorabeck CH (1989) Clin Orthop 193:247
13. Li B, Aspden RM (1997) J Bone Miner Res 641:12
14. Ding M, Dalstra M, Line F, Hvid I (1998) Acta Orthop Scand 358:69
15. Ewers BJ, Newberry WN, Garcia JJ, Haut RC (1998) Trans Orthop Res Soc 459:23
16. Li B, Aspden RM (1997) Ann Rheum Dis 247:56
17. Maudsley AA, Ernst RR (1977) Chem Phys Lett 50:368
18. Lee M, Goldburg WI (1965) Phys Rev A1261:140
19. Torchia DA (1984) J Magn Reson 613:30
20. Kim DY, Taylor HW, Moore RM, Paulsen DB, Cho DY (2003) Vet J 166:52
21. Yagi R, McBurney D, Laverty D, Weiner S, Horton WE Jr (2005) J Orthop Res 23:1128
22. Cho G, Wu Y, Ackermann JL (2003) Science 613:300
23. Wilson EE, Awomusi A, Morris MD, Kohn DH, Tecklenburg MMJ, Beck LW (2006) Biophys J 3722:90
24. Wilson MA (1987) NMR techniques and applications in geochemistry and soil chemistry. Pergamon Press, London
25. Jäger C, Welzel T, Meyer-Zaika W, Epple M (2006) Magn Reson Chem Chem 573:44